Rapid Aerostructural Optimization of Wing-Propeller Systems

Exalto, J.Q.B.; Pacini, Bernardo ; Kaneko, Shugo ; Martins, Joaquim R. R. A. ; Hoogreef, M.F.M.

DOI
10.2514/6.2024-0374

Publication date
2024

Document Version
Final published version

Published in
Proceedings of the AIAA SCITECH 2024 Forum

AIAA SciTech Forum
8-12 January 2024, Orlando, FL
AIAA SCITECH 2024 Forum

10.2514/6.2024-0374

Rapid Aerostructural Optimization of Wing-Propeller Systems

Joaquin Exalto*, Bernardo Pacini†, Shugo Kaneko‡, and Joaquim R. R. A. Martins§
University of Michigan, Ann Arbor, Michigan, United States

Maurice F.M. Hoogreef¶
Delft University of Technology, Delft, The Netherlands

Propeller-wing configurations are expected to return to the aviation industry due to their high propulsive efficiency and applicability in urban and regional air mobility. A knowledge gap exists around wing-propeller optimization because of the complexity of the propeller-wing system and the absence of a computationally efficient way to assess the coupled system. This paper addresses this gap by providing and validating a computationally efficient, mid-fidelity framework. The paper presents optimization results and recommendations for future iterations of the framework. The TU Delft PROWIM propeller is optimized with the framework, comparing sequential isolated optimization, trim optimization, and fully coupled optimization. The studies gives a conservative estimate of the efficiency gains that can be achieved by using coupled optimization, as compared to isolated optimization. Lastly, recommendations are given for future studies, such as including a battery weight model and including swirl velocities. It is expected that such model additions will affect the optimization results, and further emphasize the importance of coupled aerostructural optimization.

Nomenclature

Latin symbols

B_p	=	Number of blades per propeller (∼)
b	=	Span (m)
c	=	Wing Chord (m)
C_L	=	Lift coefficient
C_D	=	Drag coefficient (∼)
D	=	Drag (N)
G	=	Jet correction (∼)
I	=	Bessel function of first kind (∼)
J	=	Advance ratio (∼)
K	=	Bessel function of second kind (∼)
k_p	=	Propeller mass coefficient (∼)
L	=	Lift (N)
M	=	Mach number (∼)
M_{prop}	=	Spanwise propeller discretisation (∼)
M_{wing}	=	Spanwise wing discretisation (∼)
m	=	Mass (lbs)
N_p	=	Number of propellers (∼)
P	=	Power (W)
p	=	Order of bessel function (−)
R	=	Radius (m)
r_j	=	Jet radius (m)
R	=	Range (km)
T	=	Thrust (N)
V_j	=	Jet velocity (m/s)
V_0	=	Freestream velocity (m/s)
W	=	Weight (N)
x	=	Propeller location (m)

Greek Symbols

η	=	Normalized wing spanwise location
Γ	=	Circulation
μ	=	Velocity ratio
ξ	=	Normalized wing chordwise location
φ	=	Shaft power ratio
θ_{prop}	=	Propeller twist
ϕ	=	Wing Twist

Subscripts

jj	=	Panel and control point in jet
oj	=	Panel outside jet and control point inside jet
jo	=	Panel inside jet and control point outside jet
oo	=	Panel and control point outside jet

Abbreviations

AD	=	Algorithmic differentiation

*Visiting Researcher, University of Michigan—MSc, Delft University of Technology
†Ph.D. Candidate, Department of Mechanical Engineering, AIAA Student Member
‡Ph.D. Candidate, Department of Aerospace Engineering, AIAA Student Member
§Pauline M. Sherman Collegiate Professor of Aerospace Engineering, AIAA Fellow
¶Assistant Professor, Faculty of Aerospace Engineering, Kluyverweg 1, 2629HS Delft, AIAA Member

AIC	=	Aerodynamic influence coefficient	FD	=	Finite differences
APS	=	Aero-propulsive and aero-Structural	FEM	=	Finite element method
BEM	=	Blade element method	HBEM	=	Hybrid blade element method
BEMT	=	Blade element momentum theory	LB	=	Lower bound
CFD	=	Computational fluid dynamics	OAS	=	OpenAeroStruct
CS	=	Complex-step	UB	=	Upper bound
DEP	=	Distributed electric propulsion	VLM	=	Vortex lattice method
DV	=	Design variable	XDSM	=	eXtended design structure matrix
ESP	=	Equivalent specific power			

I. Introduction

The rapidly increasing socioeconomic pressure for the aviation industry to decrease its emissions requires alternative propulsion methods. Propellers offer an attractive solution. The need for more efficient aircraft and large demand for urban air vehicles (UAVs) [1], that use propellers, incentivizes research into propeller-wing design optimization. Many aerospace systems have undergone extensive optimization. However, literature on coupled propeller-wing optimization is limited, with only a few articles discussing its impact and possible benefits [2–5]. An optimization procedure for a coupled wing-propeller system could aid efficient propeller-wing designs by exploiting the coupling between the propeller and wing, and return a more efficient system than isolated optimization can.

The purpose of this paper is to present and discuss a computationally efficient framework for coupled propeller-wing optimization. The coupled system will be mid-fidelity and includes axial slipstream effects on the wing. The framework is modular such that modifying, improving, or appending modules requires minimal effort. Efficient gradient-based optimization is implemented using implicit analytic methods [6, Sec. 6.7] to compute the system's gradients. The mid-fidelity framework contains a propeller, slipstream and wing model, that are discussed in section II. The coupled system consists of a propeller code, wing code, and a slipstream model to couple the former two. The propeller, wing and slipstream code are differentiated with forward and reverse mode code, necessary for the direct and adjoint methods. The direct and adjoint methods are implicit analytic methods used to efficiently obtain a model's derivatives. Albeit efficient and accurate, implicit analytic methods require thorough verification. Model validation and derivative verification are documented in section III. The individual, and coupled, models are validated by comparing to experimental data from TU Delft's PROWIM propeller [7]. Derivative verification can be done by comparing the system's partial derivatives to derivative estimation methods such as finite differences and the complex step [8]. The optimization framework OpenMDAO [9] was used to couple the propeller, slipstream, and wing aerostructural codes. OpenMDAO is an open-source optimization framework that is particularly well-suited for gradient based optimization. The OpenMDAO architecture provides the opportunity to handle analytic derivatives, which are essential for efficient and accurate optimization.

After the models have been coupled and validated, the multidisciplinary design optimization (MDO) approach is discussed. The validated model, together with the MDO approach, are the basis for the optimization process, discussed in section VI. Sequential isolated wing- and propeller-optimizations are compared to a trimmed optimization and fully coupled optimization, such that the value of coupled wing-propeller optimization can be evaluated. It was seen that the coupled system yields a propeller power benefit of 0.8%. This results was for a small wing without battery weight and without propeller swirl velocities, which are expected to lower induced drag. Therefore, this can be considered a conservative estimate. It is expected that including battery weight further increases this number due to the snowball effect. Lastly, several model recommendations and conclusions are given.

II. Computational Method

This section addresses the computational methods used to evaluate system performance and adaptations that were necessary for optimization purposes. A schematic of the optimization architecture, called the eXtended Design Structure Matrix (XDSM) [10], is given in Figure 1. The optimizer, SNOPT [11] embedded in pyOptSparse [12], passes the propeller and wing design variables to the propeller and wing model, respectively. The slipstream model uses the velocity profile output from the propeller component to calculate a correction matrix, which is necessary to accurately predict slipstream induced lift augmentation. The wing aerostructural solver OpenAeroStruct [13] was slightly modified,

as is discussed later in this section. The wing and propeller solvers pass key variables to the objective function – the total required power – and the lift and thrust constraints.

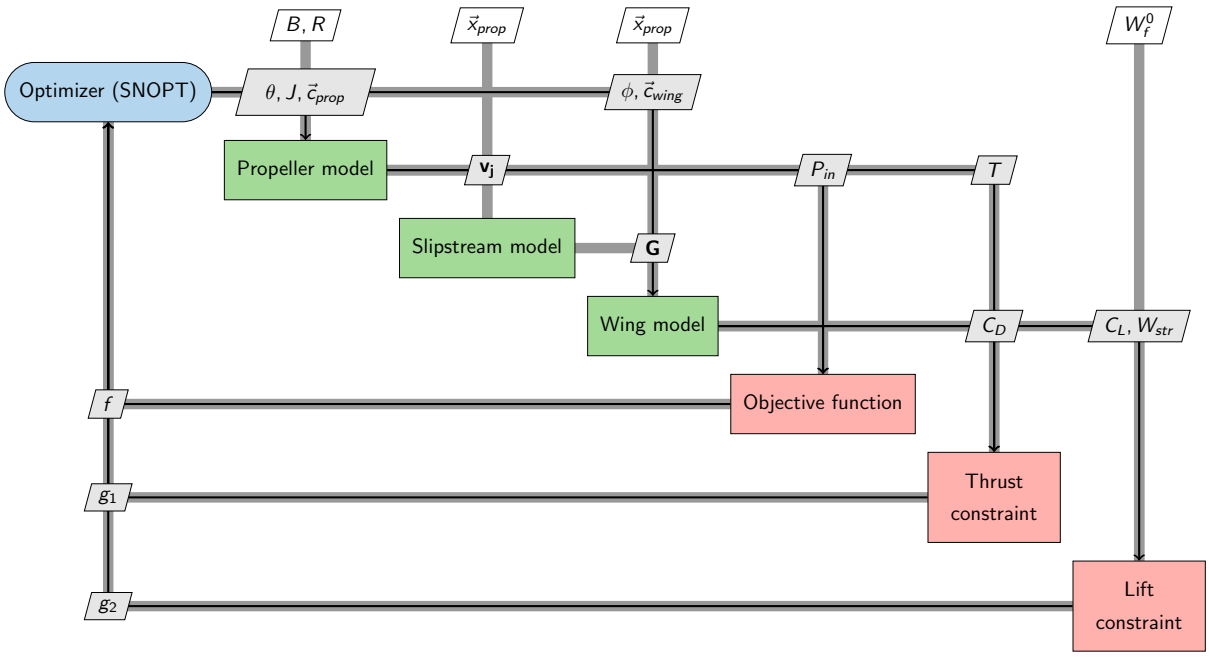

Fig. 1 The eXtended Design Structure Matrix (XDSM) for a coupled wing-propeller aerostructural optimization. The optimizer passes the design variables – wing chord and twist, and propeller rotational rate and twist – to the models. Afterwards, the propeller and wing models will pass their outputs to the constraint and objective functions.

Propeller Model

Blade element momentum theory (BEMT) is a popular method to model propeller performance because it is computationally inexpensive. BEMT is computationally efficient, yet it has enough resolution to capture the influence of the propeller geometry, which is not possible with low-fidelity disk actuator models. A BEMT code called HELIX [14] was used for this optimization framework. BEMT relies on momentum and blade element theory. Momentum theory assumes the rotor acts as an actuator disk and increases the axial momentum of the flow. Blade element theory calculates the generated thrust of each blade section. The thrust generated by each section therefore depends on the inflow conditions, blade geometry and airfoil characteristics. Furthermore, HELIX has verified forward and reverse algorithmic differentiated (AD) code that is crucial for the adjoint method [6, Sec. 6.7].

Slipstream Model

The Vortex Lattice Method (VLM) provides a popular way to model a wing at low to mid-fidelity. VLM theory is based on potential flow theory and discretizes a wing into chordwise and spanwise directions and assigns a horseshoe vortex to each panel. A VLM model cannot model wings at high angles of attack due to its inability to predict flow separation. Furthermore, VLM theory overpredicts lift when immersed in a slipstream, due to the slipstream's 'infinite' height. The infinite height is induced by the velocity vector of the VLM system, that assumes the velocity to be homogeneous. The mathematical VLM formulation is given by

$$\begin{bmatrix} AIC_{11} & \dots & AIC_{1n} \\ \vdots & \ddots & \vdots \\ AIC_{n1} & \dots & AIC_{nn} \end{bmatrix} \begin{bmatrix} \Gamma_1 \\ \vdots \\ \Gamma_n \end{bmatrix} = \begin{bmatrix} V_{\perp,1} \\ \vdots \\ V_{\perp,n} \end{bmatrix}, \tag{1}$$

where the velocity vector assumes the velocity to be homogeneous in the vertical direction, thus introducing a slipstream of infinite height. However, a slipstream has a finite height and an approximately circular shape. The classical VLM formulation cannot satisfy these boundary conditions, and returns inaccurate results. Rethorst [15] developed a correction factor that, when included, satisfies the boundary conditions of the slipstream. Rethorst's model improves the accuracy of the classical wing lifting-line model, when introduced to a velocity distribution, by reducing the lift over-prediction. The modified linear system is given by

$$\left(\begin{bmatrix} AIC_{11} & \dots & AIC_{1n} \\ \vdots & \ddots & \vdots \\ AIC_{n1} & \dots & AIC_{nn} \end{bmatrix} + \begin{bmatrix} G_{11} & \dots & G_{1n} \\ \vdots & \ddots & \vdots \\ G_{n1} & \dots & G_{nn} \end{bmatrix}\right) \begin{bmatrix} \Gamma_1 \\ \vdots \\ \Gamma_n \end{bmatrix} = \begin{bmatrix} V_{\perp,1} \\ \vdots \\ V_{\perp,n} \end{bmatrix} \tag{2}$$

The Rethorst model is based on the assumption that two velocity components exist: velocity inside, V_j, and outside, V_∞ the slipstream, with the latter being equal to the freestream velocity. In a regular lifting line model, a single boundary condition must be satisfied: the normal velocity at the panel control points should be zero. However, when a circular slipstream is introduced, two additional boundary conditions must be satisfied:

1) The pressure on each side of the jet needs to be zero, represented by $V_j u_{a,j} = V_\infty u_{a,\infty}$, where $u_{a,\infty}$ and $u_{a,j}$ are the disturbance velocity inside and outside the jet in the axial direction, respectively,.
2) Slipstream continuity needs to be satisfied, i.e. the slipstream velocity needs to be in the same direction inside and outside the jet (mathematically represented by $V_j u_{r,\infty} = V_\infty u_{r,j}$, where $u_{r,j}$ and $u_{r,\infty}$ are the disturbance velocity inside and outside the jet in radial direction, respectively).

To satisfy these boundaries conditions, a correction matrix is added to the AIC matrix, denoted by G_{ii} in Equation (2). The correction factor is equivalent to including mirror vortices that satisfy the boundary conditions at the slipstream. The method has a number of similarities with the 'wing near a solid surface'-method: when a wing is near a solid surface, mirror vortices 'in' the solid surface satisfy the boundary conditions at the solid surface. Rethorst splits the mirror vortices into an even and odd solution. The even and odd equations are split into four distinct parts. Whether the control points and vortices are inside or outside the jet determines which equation is used. The distinction between equations is indicated in the subscript of the equations. The first letter of the subscript indicates whether the control point is inside (j) or outside (o) the jet, and the second letter indicates whether the vortex is inside or outside the jet. The second level subscript —e or o —indicates whether the equations represent the even or odd solution. The full set of eight equations is given in Equations (3)– (10). In Equations (3)– (10), r_j represents the jet radius, $\eta = y/r_j$ is the normalized spanwise location, $\chi = x/r_j$ is the normalized chordwise location, and $\mu = V_j/V_\infty$ is the ratio of slipstream versus freestream velocity. The variables c and d are the locations of the edges of the horseshoe vortices. The odd solution uses modified Bessel functions of the first and second kind - I and K, respectively—and their derivatives—I', K'. The Bessel functions are of order $2p + 1$ and the integrals use running variable λ. A convergence study by Nederlof [16] showed that having λ run from 0 to 20 and using $p = 5$, for the Bessel function order $2p + 1$, as an upper boundary is sufficient to have the system converge.

$$G_{jj_{\text{even}}}(\chi) = \frac{1-\mu^2}{5\cdot(1+mu^2)}\left[\frac{1}{1/f-\chi} - \frac{1}{1/e-\chi} + \frac{1}{1/f+\chi} - \frac{1}{1/e+\chi}\right] \tag{3}$$

$$G_{oj_{\text{even}}}(\chi) = \frac{(1-\mu)^2}{5\cdot(1+mu^2)}\left[\frac{1}{\chi-e} - \frac{1}{\chi-f} + \frac{1}{f+\chi} - \frac{1}{e+\chi}\right] \tag{4}$$

$$G_{jo_{\text{even}}}(\chi) = -G_{oj_{\text{even}}}(\chi) \tag{5}$$

$$G_{oo_{\text{even}}}(\chi) = -G_{jj_{\text{even}}}(\chi) \tag{6}$$

$$G_{jj_{\text{odd}}}(\chi,\ \xi) = \frac{8}{5\pi\chi}\sum_{\upsilon}^{\infty}(2\upsilon+1)^2\int_0^\infty \frac{K_\upsilon K_\upsilon' I_\upsilon(\xi\chi)\sin(\xi\chi)}{[1/(1/\mu^2)-1]-\lambda I_\upsilon K_\upsilon'}\int_{e\lambda}^{f\lambda}\frac{I_\upsilon\lambda_\beta}{\lambda_\beta}d\lambda_\beta d\lambda \tag{7}$$

$$G_{oj_{\text{odd}}}(\chi,\ \xi) = \frac{8}{5\pi\chi}\sum_{\upsilon}^{\infty}(2\upsilon+1)^2\int_0^\infty \left[\frac{1}{\mu-\lambda(1/\mu-\mu)I_\upsilon K_\upsilon'}\right]\frac{K_\upsilon(\chi\lambda)\sin(\xi\lambda)}{\lambda}\int_{e\lambda}^{f\lambda}\frac{I_\upsilon\lambda_\beta}{\lambda_\beta}d\lambda_\beta d\lambda \tag{8}$$

$$G_{jo_{\text{odd}}}(\chi,\ \xi) = \frac{8}{5\pi\chi}\sum_{\upsilon}^{\infty}(2\upsilon+1)^2\int_0^\infty \left[\frac{1}{\mu-\lambda(1/\mu-\mu)I_\upsilon K_\upsilon'}\right]\frac{K_\upsilon(\chi\lambda)\sin(\xi\lambda)}{\lambda}\int_{e\lambda}^{f\lambda}\frac{I_\upsilon\lambda_\beta}{\lambda_\beta}d\lambda_\beta d\lambda \tag{9}$$

$$G_{oo_{\text{odd}}}(\chi,\ \xi) = \frac{8}{5\pi\chi}\sum_{\upsilon}^{\infty}(2\upsilon+1)^2\int_0^{\infty}\frac{K_\nu K_\nu\prime I_\nu(\xi\chi)\sin(\xi\chi)}{[1/(1/\mu^2)-1]-\lambda I_\nu K_\nu\prime}\int_{e\lambda}^{f\lambda}\frac{I_\nu\lambda_\beta}{\lambda_\beta}d\lambda_\beta d\lambda \tag{10}$$

Several authors (Willemsen [17], Nederlof [16, 18], and van der Leer [19]) have used the Rethorst correction in their studies and have verified the numerical results by comparing to either CFD (Willemsen [17], Nederlof [16]) or experimental (van der Leer [19]) data. However, before the Rethorst model can be used, its requirements (and limitations) must be identified. The model limitations are given below, together with a solution if the limitations pose an issue:

- The Rethorst model requires the slipstream to be in the center of the wing, the center of the slipstream to be aligned with the center of a VLM panel, and the slipstream edges to be aligned with VLM panels. The wing-mesh is therefore formed around the propellers. However, it is important for the VLM to have panels, inside and outside the slipstream, with approximately the same size. Therefore, the number of panels inside and outside the propeller should be carefully chosen such that the ratio is as close to one as possible. An example of a wing mesh is visualized in Figure 2.
- Wing-tip propellers violate all of the above requirements due to their location, and thus render Rethorst's correction unusable. However, as Willemsen [17] showed, the wing can be extended with an 'imaginary' part which is later neglected. Willemsen showed that the method is accurate, judging by a validation against experimental data, from the TU Delft PROWIM propeller [7].
- The odd solution, given by Equations (7)–(10), is expensive to calculate due to several Bessel functions inside nested integrals. The odd solution of the Rethorst correction crippled the framework's computational efficiency. Nederlof [16] found that limiting the Rethorst correction to its inexpensive even equations yields reasonable results. More efficient algorithms for converging Bessel function exist but have not been implemented: Algorithm 644 by D.E. Amos [20].
- The propeller introduces a velocity distribution, where Rethorst assumes a velocity step increment. Van der Leer and Hoogreef [19] and Prabhu [21] showed that the Rethorst correction is suitable for super positioning: combining several slipstreams, varying in diameter and velocity increment, or decrement, creates a velocity distribution.

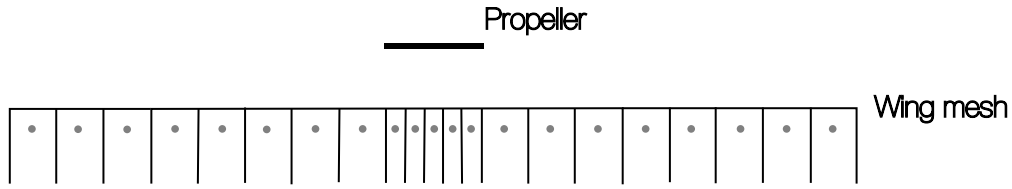

Fig. 2 Visualization of wing-meshing required for Rethorst method. The panels inside the slipstream are much smaller than those outside for visualization purposes. In reality these panels are approximately the same size.

Wing model

The wing is modeled using the open-source code OpenAeroStruct [13] (OAS). Minor modifications were necessary to include the Rethorst correction matrix and the velocity distribution, since uniform inflow is assumed in the unaltered version of OAS. Additionally, a new meshing function was added, to guarantee propeller and VLM mesh alignment. For the VLM it is critical to ensure the panels behind the wing and propeller are approximately the same size. If the ratio between these two panels varies too significantly, the optimization results are less smooth. The aerodynamic wing-model uses a VLM with one panel in the chordwise direction, otherwise called a Weissinger VLM. We chose a Weissinger VLM because the errors of the slipstream model grows as the wing is discretised in the chordwise direction. The uncertainty of the slipstream model grows with chordwise discretisation since the odd solution in the Rethorst method is neglected. This assumption is in line with previous literature that uses the Rethorst method [16–18, 22] but should be noted as a model-limitation. A Weissinger VLM is shown in Figure 3, as taken from Nederlof [18].

Parasitic drag is calculated in OAS by using skin friction and form-factor formulas found in Raymer [23]. Furthermore, OAS uses the Von Mises stress in combination with the material failure criteria to assess structural integrity. For the structural model a tubular structural element is used. The tubular structural model assumes all loads are carried by a tube inside the wing. This approximation is considered valid since the framework aims for mid-fidelity. A wing-box model could also be included in future iterations of the framework. Each structural node in the tubular spar model

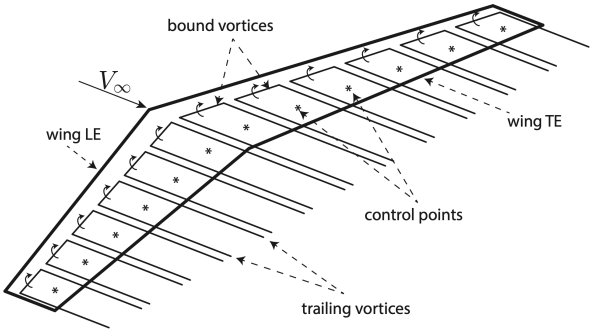

Fig. 3 Drawing of Weissinger VLM, from Nederlof [16], with permission

has a Von Mises stress value. If one performs analyses, choosing the node with the maximum stress value would be sufficient to assess structural integrity. However, a `max`-function introduces a non-smooth constraint function. A non-smooth constraint function could corrupt the optimization process as it introduces discontinuities. To prevent a potential discontinuous constraint function, an aggregated failure constraint is used. The Kreisselmeier–Steinhauser (KS) function was used to aggregate the individual elemental failure constraints [6, 24]. Using the KS function decreases the number of constraints in an optimization problem by combining them into a single or multiple constraint functions. The KS function returns a smoother constraint function, as compared to only using a max function, and thus produces a better posed optimization problem. OAS calculates C_L by dividing the lift force by $0.5\rho V_\infty^2 A_{\text{wing}}$. However, the wing-propeller system does not see V_∞, but V_{eff} since the wing experiences a velocity distribution. Therefore, the C_l- and C_L-calculations use V_{eff}, which is the averaged velocity. $\mathbf{C}_l$ and C_L are given by

$$\mathbf{C}_l = \frac{l}{(0.5\rho V_{\text{eff}}^2 c_{\text{local}} s_{\text{local}})} \tag{11}$$

$$C_L = L/(0.5\rho V_{\text{eff}}^2 A_{\text{wing}}), \tag{12}$$

where c_{local} is the local chord, s_{local} is the length of the spanwise element, and A_{wing} is the total wing area. Lastly, OAS iterates on the aerodynamic load and structure deformation. A block Gauss-Seidel converges this feedback loop; the induced aerodynamic load is calculated, which thereafter deforms the wing, which subsequently changes the induced aerodynamic load.

III. Model Verification and Validation

Model validation was carried out using the TU Delft PROWIM propeller used in studies by Veldhuis [25] and Sinnige [7]. The TU Delft PROWIM propeller was configured in tractor configuration in previous work by Sinnige. The PROWIM setup parameters are shown below.

Table 1 PROWIM setup data

Parameter	Value
Radius	0.1185 m
Hub Radius	0.03496 m
Span	0.73 m
Chord	0.24 m
Wing thickness	0.036 m
Propeller location	0.332 m

The propeller code HELIX can be validated by comparing numerical and empirical data for the thrust- and power-coefficients versus advance ratio, shown in Figure 4. The slope of the numerical and experimental coefficients

are largely similar. However, a discrepancy can be noted in the magnitude of the thrust coefficient. The numerical model has the tendency to slightly over-predict the thrust coefficient. A reason for this could be the geometry of the inboard sections of the PROWIM propeller. The PROWIM's inboard section are circular and thus generate negative thrust. This negative thrust is not accounted for in HELIX, thus it is expected that the thrust calculations experience an over-estimation, especially at large advance ratios. Other effects that are not modeled, such as spanwise velocity components, could also contribute to the disparity between numerical and experimental results. Lastly, the absence of a nacelle is also expected to have an impact on the accuracy of the numerical model.

The wing-propeller validation results are shown in Figure 5. The numerical and experimental data have a good fit. At zero rotational speed, i.e. $J = \infty$, there is a disparity between the numerical and experimental data. A cause of this discrepancy could be the limited chordwise discretisation of the wing in the VLM. This disparity is translated to the lower advance ratios as well and should be considered when assessing results. The numerical and experimental data see the largest offset at higher angles of attack. The disparity for the wing-propeller model at high angles of attack is expected since VLMs are incapable of accurately modeling separation, that becomes more important as the angle of attack increases.

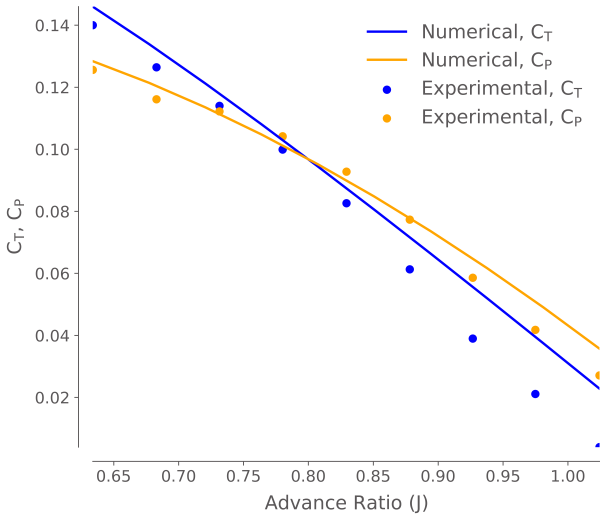

Fig. 4 Comparison of thrust- and power-coefficients between numerical (HELIX [14]) and experimental propeller performance data

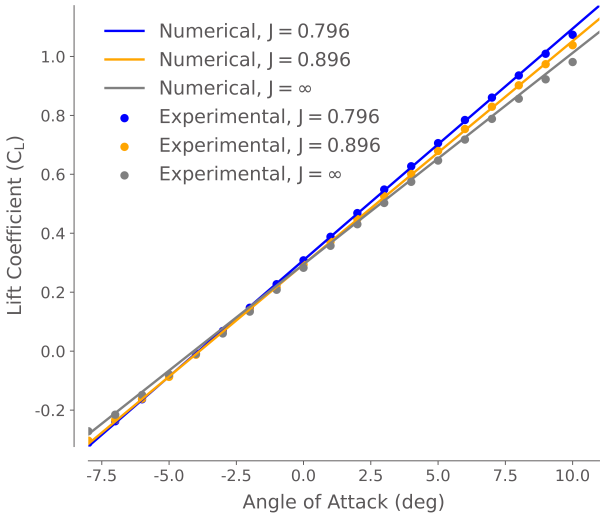

Fig. 5 Numerical and experimental [7] results of the PROWIM setup

The isolated propeller and wing and coupled wing-propeller models return data that shows good resemblance with experimental data. At higher advance ratios the propeller model might over-predict thrust. The propeller power numerical data seems to match experimental data well throughout the advance ratio spectrum. These considerations are important when assessing the optimization results.

IV. Multidisciplinary Design Optimization

Gradient based optimization can drastically improve accuracy and decrease computational overhead of an optimization process, compared to gradient-free methods [26]. To perform gradient-based optimization, the gradient of the objective function and constraints need to be determined, given in Equations (13) and (14), respectively.

$$\frac{\partial f}{\partial \mathbf{x}} : \text{ Objective function gradient} \tag{13}$$

$$\frac{\partial \mathbf{g}}{\partial \mathbf{x}} : \text{ Constraint Jacobian} \tag{14}$$

The objective function and constraint gradients can be obtained by treating the coupled model as a black box and using finite differences (FD). A finite difference scheme is easy to implement and complex model details do not have to be considered to obtain derivatives. However, finite differences are often inaccurate [6, Sec. 6.7] and scale linearly, thus poorly, with an increase in design variables. The (forward) finite difference scheme for the objective function is given by

$$\frac{\partial f}{\partial x_i} = \frac{f(\mathbf{x} + \Delta x_i) - f(x)}{\partial x_i}. \tag{15}$$

Next to finite differences, derivatives can also be obtained by using the complex step method. CS is similar to finite differences, since it uses an increment to assess a derivative. However, CS takes the step into the complex domain. This approach yields a higher accuracy since the truncation error now scales with h^2 and there is subtraction error [8]. Algorithmic differentiation (AD) rewrites a source-code to output the model derivatives. AD uses two implementations: forward and reverse. Forward AD runs the differentiated code from input to output. Similar to FD and CS, forward-AD code is run once for each design variable and returns the derivatives. Reverse AD is advantageous when more inputs than outputs exist. Reverse AD runs the code in forward mode once, after which the code is run in reverse to obtain the derivatives of the inputs with respect to the outputs. However, neither FD, CS, or AD are efficient since they requires solving the governing equations for each derivative. Implicit analytic methods do not require iteratively solving the governing equations and can therefore improve the efficiency of derivative computation [26]. The functions of interest, and system residuals, are written as Equations (16) and (17), respectively.

$$f = f(\mathbf{x}, \mathbf{u}(\mathbf{x})) : \text{ Objective function} \tag{16}$$

$$r(\mathbf{x}, \mathbf{u}(\mathbf{x})) = 0 : \text{ Residuals function} \tag{17}$$

Consequently, the total derivative is written as:

$$\frac{\mathrm{d}f}{\mathrm{d}\mathbf{x}} = \frac{\partial f}{\partial \mathbf{x}} + \frac{\partial f}{\partial u}\frac{\mathrm{d}\mathbf{u}}{\mathrm{d}\mathbf{x}}. \tag{18}$$

Total derivatives, indicated by d, require solving the governing equations, and are thus computationally expensive, whilst partial derivatives, denoted by ∂ do not. The residual equation is expressed similarly to Equation (18), rearranged for $\frac{\mathrm{d}r}{\mathrm{d}\mathbf{x}} = 0$:

$$\frac{\mathrm{d}r}{\mathrm{d}\mathbf{x}} = \frac{\partial r}{\partial \mathbf{x}} + \frac{\partial r}{\partial u}\frac{\mathrm{d}\mathbf{u}}{\mathrm{d}\mathbf{x}} \rightarrow \frac{\mathrm{d}\mathbf{u}}{\mathrm{d}\mathbf{x}} = -\left[\frac{\partial r}{\partial \mathbf{u}}\right]^{-1}\frac{\partial r}{\partial \mathbf{x}}. \tag{19}$$

Substituting $\mathrm{d}\mathbf{u}/\mathrm{d}\mathbf{x}$ into Equation (19) gives:

$$\frac{\mathrm{d}f}{\mathrm{d}\mathbf{x}} = \frac{\partial f}{\partial \mathbf{x}} - \underbrace{\frac{\partial f}{\partial \mathbf{u}}}_{\psi^T}\overbrace{\left[\frac{\partial \mathbf{r}}{\partial \mathbf{u}}\right]^{-1}}^{\phi}\frac{\partial \mathbf{r}}{\partial \mathbf{x}}. \tag{20}$$

The adjoint method [6, Sec. 6.7] solves for ψ, where the direct method solves for ϕ. The cost of the adjoint method is proportional to the number of functions of interest, where the cost of the direct method is proportional to the number of design variables, similar to reverse- and forward-AD. Forward or reverse AD are used to calculate the partial derivatives. Computing derivatives analytically or with AD does require the derivatives to be verified since wrong derivatives could lead the optimizer to wrong designs. Derivative verification starts by calculating finite differences. Subsequently, the finite differences are used to verify the complex step derivatives [8]. Afterwards, the partial derivatives returned by forward- and reverse-AD are verified using the complex step derivatives.

The total derivatives of the output functions, namely; wing failure, lift equal to weight, thrust equal to drag, and the objective function propeller power with respect to the inputs propeller rotational speeds, propeller locations, propeller radii, wing chord and wing twist must be verified. Table 2 details the largest relative errors of each output's derivative. The total derivatives are checked with respect to central finite differences. Furthermore, the derivatives of the propeller and slipstream code are perfectly symmetrical. Meaning that the relative error for the design variables of the left propeller are the same as for the right propeller. The largest of these relative errors for the total derivatives is on the order of 10^{-2}. The failure derivative with respect to rotational rate is in the order of 10^{-10}. Finite differences is plagued by finite numerical precision issues. It is likely that the verification value, retrieved using FD, is corrupted by finite precision and that the AD derivative is correct. Therefore, it can be stated that all model outputs, constraints, and objective functions derivatives with respect to the inputs are verified, meaning the architecture can be assumed mathematically correct.

Table 2 Total derivative verification

Function	Variable	Adjoint	FD Deriv.	Relative error
Propeller power	Rotational rate propeller	1.9667	1.9667	$2.9441 \cdot 10^{-7}$
$L - W = 0$	Rotational rate propeller	$2.1579 \cdot 10^{-6}$	$2.1581 \cdot 10^{-6}$	$1.1149 \cdot 10^{-4}$
$T - D = 0$	Wing thickness	$1.4688 \cdot 10^{-5}$	$1.4687 \cdot 10^{-5}$	$1.7460 \cdot 10^{-4}$
Wing structural failure	Rotational rate propeller	$3.5350 \cdot 10^{-10}$	$3.4925 \cdot 10^{-10}$	$1.2191 \cdot 10^{-2}$
Wing $C_{L,max}$	Wing thickness	$5.6118 \cdot 10^{-6}$	$5.6118 \cdot 10^{-6}$	$1.9754 \cdot 10^{-4}$
Intersection	Wing chord	$1.1965 \cdot 10^{-1}$	$1.1965 \cdot 10^{-1}$	$1.5983 \cdot 10^{-9}$

V. Optimization Formulations

The optimization statement for the wing-propeller optimization is given by

$$\begin{aligned} \min_{\mathbf{x}} \quad & P_{\text{prop}} \\ \text{s.t.} \quad & T(\mathbf{x}) - D(\mathbf{x}) = 0 \\ & L(\mathbf{x}) - W(\mathbf{x}) = 0 \\ & C_L(\mathbf{x}) \leq 0.8 \\ & \text{Failure}(\mathbf{x}) < 0 \\ & \text{Intersects}(\mathbf{x}) < 0, \end{aligned} \tag{21}$$

and the design vector is elaborated on in Table 3. The coupled wing-propeller optimization shall minimize the required propeller power, whilst constrained by lift equaling weight, thrust equaling drag, and the structural integrity of the wing. Furthermore, some additional constraints – such as the thickness and intersect constraints – are required to prevent the optimizer from exploiting infeasible designs. The structural failure constraint guarantees structural integrity by assessing the structure's properties and the induced load on the wing. The structural model uses a tube model, which is valid for small wings [13], but requires an additional constraint to prevent intersection of the outer and inner radii, as is given in the last line of Equation (21). The yield stress is divided by 2.5 to simulate a situation in which the wing experiences a load higher than during cruise, which could happen during a manoeuvre.

The optimization is performed during cruise, which calls for lift to weight and thrust to drag constraints. Additionally, C_L should be constrained to a maximum value, since a VLM is not capable of modeling flow separation. A VLM might naturally tend to high C_L values by increasing the twist, to satisfy the $L = W$ constraint. However, at such high angles of attack flow separation occurs, not modeled by a VLM, thus rendering the lift estimation inaccurate. Furthermore, stall could suddenly occur at high angles of attack. Therefore, the C_L constraint also serves as a safety margin to prevent stall. $C_{L,max} = 0.8$ was chosen based on literature [27].

The design variables are summarized as vector $\mathbf{x}$, that is detailed in Table 3, where N_{prop} is the number of propellers, H_{prop} is the number of propeller discretisation points, and H_{wing} is the number of wing discretisation points.

Table 3 Elements of optimization design vector, x

Design variable	Symbol	Unit	Size
Propeller twist	θ_{prop}	deg	$N_{\text{prop}}; M_{\text{prop}}$
Propeller advance ratio	$\mathbf{J}_{\text{prop}}$	-	N_{prop}
Wing chord	$\mathbf{c}$	m	M_{wing}
Wing twist	ϕ	deg	M_{wing}
Wing thickness	t	m	M_{wing}

Section VI discusses isolated wing, isolated propeller, and coupled wing-propeller optimization. The former two are a simplified version of the coupled optimization. The optimization statement for isolated wing and propeller

optimization are given by Equation (22) and Equation (23), respectively. The design vector for the wing optimization contains $\mathbf{x}_{\text{wing}} = [\phi,\ \mathbf{c},\ t]$, where the propeller optimization has design vector $\mathbf{x}_{\text{prop}} = [\theta_{\text{prop}},\ \mathbf{J}_{\text{prop}}]$.

$$\begin{aligned} \min_{\mathbf{x}_{\text{wing}}} \quad & D = D_i + D_v \\ \text{s.t.} \quad & L(\mathbf{x}_{\text{wing}}) = W(\mathbf{x}_{\text{wing}}) \\ & C_L(\mathbf{x}_{\text{wing}}) < 0.8 \\ & \text{Failure}(\mathbf{x}_{\text{wing}}) < 0 \\ & \text{Intersects}(\mathbf{x}_{\text{wing}}) < 0 \end{aligned} \tag{22}$$

$$\begin{aligned} \min_{\mathbf{x}_{\text{prop}}} \quad & P_{\text{prop}} \\ \text{s.t.} \quad & T(\mathbf{x}_{\text{prop}}) = T_0(\mathbf{x}_{\text{prop},0}) \end{aligned} \tag{23}$$

VI. Optimization Results and Discussion

This sections discusses the differences between isolated wing- and propeller-optimization and the coupled optimization. The baseline configuration used for optimizations is the TU Delft PROWIM wing and propeller. For the coupled optimization, the isolated optimization designs are used as an initial configuration. The parameters used for the optimizations are given in Table 4.

Table 4 Elements of optimization design vector, x

Parameter	Value	Unit
α	2.0	deg
m_0	4.0	kg
$C_{D,0}$	$2.5{\cdot}10^{-2}$	-
$C_{L,0}$	0.0	-
V_∞	40.0	m/s
ρ_∞	1.20885	kg/m^3
Re	$3.5{\cdot}10^5$	-

Isolated Wing Optimization

The isolated wing optimization statement is given in Equation (22). The twist and chord are both decreased near the tips, as shown in Figure 6. The optimized chord is at about 25% of the original chord, with a slight increase near the center of the wing. Minimizing chord reduces the viscous drag, as is expected. The twist distribution can afterwards augment the lift distribution to approach an elliptical lift distribution. Furthermore, the weight of the structure was decreased by decreasing the tube thickness, whilst guaranteeing structural integrity: the thickness variable hit its lower bound at 3 mm across the wingspan. Lastly, the initial wing was a straight wing that produced significantly more lift than required according the the lift equals weight constraint.

The lift distribution is shown in Figure 6. The black dashed curve shows an elliptical lift distribution. The optimized design approaches an elliptical lift distribution. However, where aerodynamic optimization would produce an elliptical lift curve, aerostructural optimization might prefer a different lift distribution. The optimization process attempted to minimize the drag, while constraining lift equal to weight. Decreasing the weight reduces the required lift, and subsequently drag. Therefore, minimizing the structural weight is important. Additionally, the failure constraint was active at the optimized configuration. Decreasing the loads further from the center of the wing, and increasing the load at the center, decreases the bending moment. Therefore the aerodynamic load towards the tips is lower than the aerodynamically optimal elliptical distribution. These results are in line with other aerostructural wing optimization studies [13, 28].

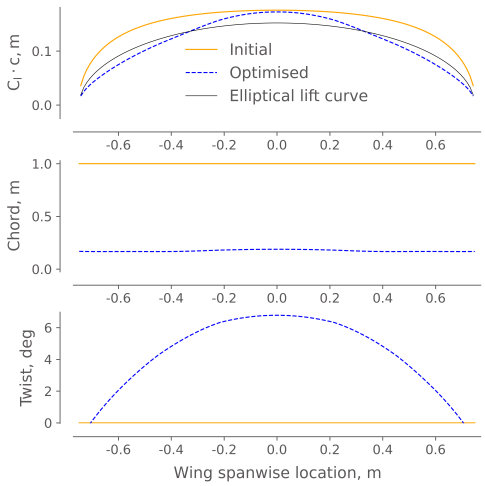

Fig. 6 Lift, twist, and chord distributions for baseline wing and isolated wing optimization

Table 5 Isolated wing optimization results

Outputs	Initial	Optimized
L (N)	$5.1979 \cdot 10^{1}$	$8.67147 \cdot 10^{1}$
D (N)	9.8182	$1.04926 \cdot 10^{1}$
$1 - \frac{L}{W} = 0$ (-)	$5.77017 \cdot 10^{-1}$	$-8.495 \cdot 10^{-13}$
Failure (-)	$-9.0 \cdot 10^{-1}$	$1.3278649 \cdot 10^{-12}$

Isolated Propeller optimization

For the isolated propeller optimization, the TU Delft PROWIM [7] propeller is used as a baseline design. The isolated propeller optimization statement is given in Equation (23), where the design variables, **x**, comprise of the rotational velocity J, and blade twist θ_{prop}.

The optimized isolated propeller twist distribution and the velocity distribution are shown in Figure 7. The optimizer preferred a propeller with a smooth velocity distribution. Furthermore, the rotational rate was significantly decreased, as is seen in Table 6. A smoother velocity distribution is to be expected, since it reduces the amount of vorticity, and consequent losses. Furthermore, the velocity, and thus force, distribution is moved inboard. Moving the force distribution inboard decreases the moment arm and thus torque. Lowering the torque consequently also decreases propeller power, as is the objective of the optimization.

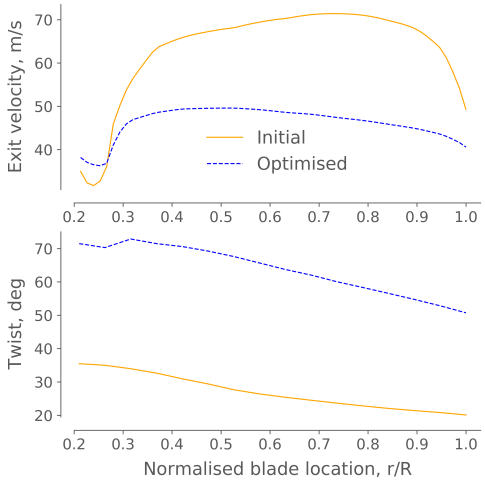

Fig. 7 The propeller twist (top) and velocity distribution (bottom)

Table 6 Isolated propeller optimization results

DV (unit)	LB	Initial	UB	Optimized
Rotational rate (rpm)	0	1060	3000	491.7
Outputs		**Initial**		**Optimized**
Power (W)	-	433.1	-	194.2
Thrust (N)	-	4.582	-	4.582

Trimmed and Coupled Wing-Propeller Optimization

The coupled wing-propeller optimization used the same PROWIM setup as the isolated wing and propeller optimization setups. The trimmed analysis starts from the isolated propeller and wing optimization designs. Afterwards it is given the freedom to modify the wing angle of attack and propeller rotational rate. The trimmed system must

satisfy the constraints, but cannot change the propeller and wing designs. Comparing the trim results to the coupled optimization results shows the importance of multidisciplinary design optimization. An XDSM of the trimmed analysis is given in Figure 8.

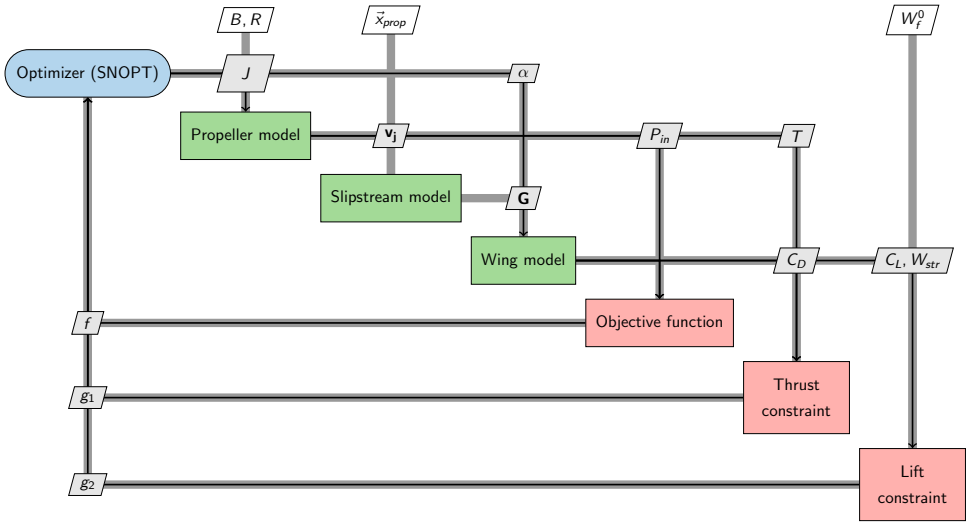

Fig. 8 An XDSM explaining the trim process. The trim optimization satisfies the constraints by changing the advance ratio and wing angle of attack. However, it is not able to change the propeller or wing designs.

The coupled wing-propeller system optimization procedure minimized the propeller power, whilst constraining thrust to be equal to drag, lift equal to weight and the structural integrity of the wing had to be guaranteed. The optimization statement is given in Equation (21).

Table 7 Results of the coupled wing-propeller optimization, the results for both propellers were identical to the fifth decimal therefore only one is given. Trimmed analysis guarantees the thrust and drag constraints to be satisfied by varying the propeller rotational rate and wing angle of attack. Fully coupled optimization can modify design variables to redesign the propeller and wing designs for the new operating conditions.

Design Variable (units)	LB	Initial	UB	Isolated sequential	Trimmed coupled	Fully coupled
Rotational speed (rad/s)	0	$1.060{\cdot}10^{3}$	3000	$2.450 \cdot 10^{2}$	$2.446 \cdot 10^{2}$	$2.445 \cdot 10^{2}$
Thickness (m)	0.003	$1.0{\cdot}10^{-2}$	0.5	$3.0 \cdot 10^{-3}$	$3.0 \cdot 10^{-3}$	$3.0 \cdot 10^{-3}$
Angle of Attack (deg)	-8.0	$2.0{\cdot}10^{0}$	8.0	$2.0 \cdot 10^{0}$	$1.469 \cdot 10^{0}$	$2.0 \cdot 10^{0}$
Results						
Failure (-)	–	$-9.441{\cdot}10^{-1}$	0.0	$-1.146 \cdot 10^{-10}$	$-2.713 \cdot 10^{-3}$	$4.901 \cdot 10^{-5}$
min(Intersects) (-)	–	$-1.15{\cdot}10^{-2}$	0.0	$-3.223 \cdot 10^{-4}$	$-1.909 \cdot 10^{-4}$	$-3.635 \cdot 10^{-4}$
$1 - L/W = 0$ (-)	0.0	$4.118{\cdot}10^{-1}$	0.0	$-5.0544 \cdot 10^{-5}$	$-2.7546 \cdot 10^{-9}$	$-2.7546 \cdot 10^{-6}$
$1 - T/D = 0$ (-)	0.0	$-1.166{\cdot}10^{0}$	0.0	–	$-2.757 \cdot 10^{-6}$	$3.540 \cdot 10^{-5}$
$Thrust$ (N)	–	$4.582{\cdot}10^{0}$	–	$1.330 \cdot 10^{0}$	$1.325 \cdot 10^{0}$	$1.325 \cdot 10^{0}$
D (N)	–	$4.2575{\cdot}10^{0}$	–	$2.667 \cdot 10^{0}$	$2.647 \cdot 10^{0}$	$2.646 \cdot 10^{0}$
L (N)	–	$4.380{\cdot}10^{1}$	–	$4.162 \cdot 10^{1}$	$4.162 \cdot 10^{1}$	$4.162 \cdot 10^{1}$
m_{struc} (kg)	–	$2.594{\cdot}10^{0}$	–	$2.440 \cdot 10^{-1}$	$2.440 \cdot 10^{-1}$	$2.440 \cdot 10^{-1}$
C_L (-)	–	$1.358{\cdot}10^{-1}$	–	$7.489 \cdot 10^{-1}$	$7.383 \cdot 10^{-1}$	$7.490 \cdot 10^{-1}$
P (W)	–	$4.331{\cdot}10^{2}$	–	$1.1314 \cdot 10^{1}$	$1.1234 \cdot 10^{2}$	$1.1228 \cdot 10^{2}$

Table 7 lists the isolated and coupled optimized system results. The coupled system produces exactly the same amount of lift as the trimmed and isolated system, since the structural weight remained constant as well. The trimmed

and optimized systems show a power decrease as compared to the isolated optimization, thus signifying the importance of coupled models, and coupled optimization. The coupled system however can achieve a slightly lower drag value by decreasing the wing twist. The lower drag value decreased the required thrust, and thus propeller power. The benefit of coupled multidisciplinary optimization with the current model is a power decrease of 0.8%. This number is expected to be a conservative estimate, because weight models and propeller wake models that can estimate the decrease in induced drag are not included.

The wing twist and chord distribution of the optimized coupled and isolated wing are shown in Figure 9. Generally the twist and chord distributions follow the same trend. However, the wing twist near the propeller is slightly reduced. The optimizer reduces the twist at this location because the propeller augments the lift at that section. The chord distribution is nearly identical between the coupled and isolated optimizations, with a very subtle increase around the center to accommodate for the structure. The lift distribution decreases the load near the tips, to minimize structural weight, and sees an increase at roughly where the left propeller starts, to where the right propeller ends. Increasing the lift between the propellers makes sense since the presence of the propeller increases the lift, thus the optimizer attempts to exploit this benefit.

The coupled system returns an optimized propeller that shows similarities with the isolated optimized propeller. However, the coupled propeller optimization does show an interesting oscillation in propeller twist, and thus velocity. The propeller passes the propeller wake velocity at predetermined points to the wing. Those points correspond with where peaks are seen in the velocity distribution. The local peaks cause the wing to experience a higher velocity propeller induced velocity. Refining the wing discretisation decreases this effect. However, highly refined wing meshes performed much worse in the aerostructural solver. Therefore, this is an important model limitation that is not physical and could be addressed with a smoothing function. A coupled optimization without propeller twist as a design variable was run to guarantee that these oscillations were not significantly impacting the optimization outcome. The simulation returned a power of $p = 112.29\ W$; a 0.0089% difference, showing the negligible benefit that these oscillations provide.

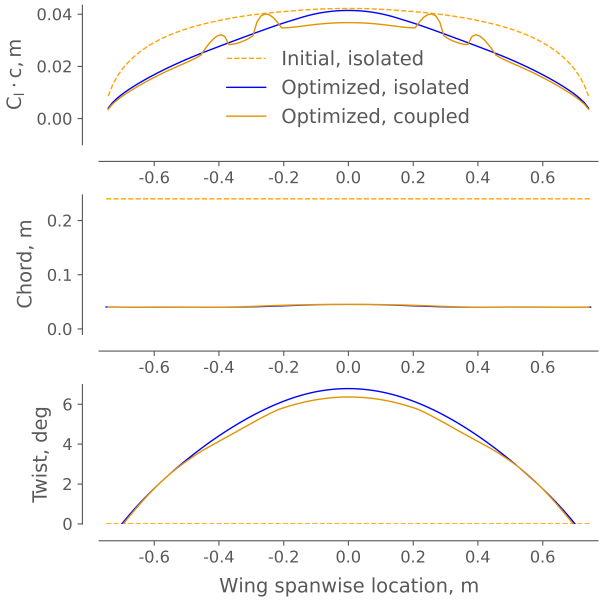

Fig. 9 The wing lift, twist and chord distribution

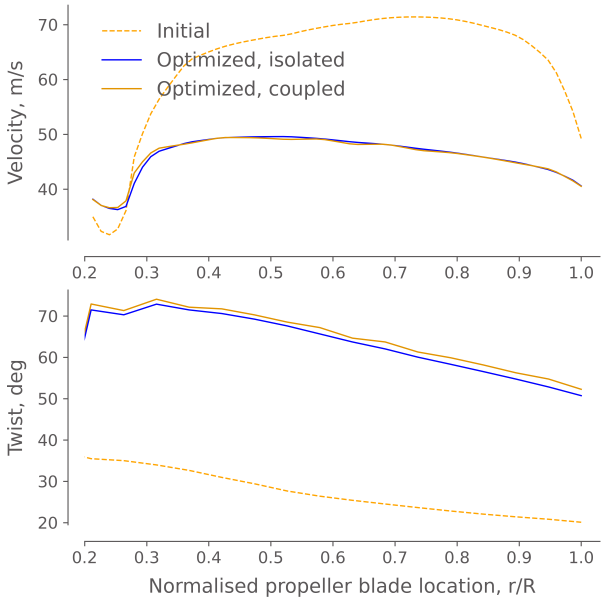

Fig. 10 The prop twist and velocity distribution

Coupled wing-propeller optimization provides more relevant results for a wing-propeller system than isolated wing- and propeller-optimization. Wing-propeller system design is inherently a coupled design procedure, since the performance of one affects the other. The lift augmentation due to the propeller's presence decreases the wing size, thus lowering structural mass and the lift equals weight constraint. Consequently, the drag, and thus thrust constraint, decreases. Lowering the thrust constraint changes the optimized propeller design. Including this feedback loop therefore returns more relevant results when designing a propeller-wing system than combining isolated wing- and propeller-optimization results. As of now the benefit is in the order of 0.8%, which might seem like a small difference. However, 0.8% is a conservative estimate, since the propeller induced down-wash was not modeled, nor

were the radius and location optimized. The down-wash will reduce the induced drag, consequently lowering the required propeller power. Therefore, the required thrust can be lowered. The propeller power is closely related to the thrust constraint, and the coupled optimization redesigns the propeller for lower input power at the new operating condition.

The propeller-wing optimization process also showed important propeller-wing model coupling properties. Coupling a wing to a propeller affects the optimization process because not all propeller blade discretisation point are translated to the wing. The consequence of this limitation is that the propeller blade design experiences the oscillations that can be seen in Figure 10. Therefore only the locations that translate their velocity to the wing see an increase in propeller velocity output, where others see a decrease, likely to reduce propeller power.

VII. Model Recommendations

The current model includes propeller-wing coupling in a relatively simplistic way: the propeller induced axial momentum is translated to the wing. In reality, propeller-wing interaction is much more complicated. This section discusses some of the effects that are currently not included and could aid the optimization procedure. A requirement for any additional models is that they must be computationally efficient. Modeling propeller-wing interaction with high fidelity is possible using CFD-based methods. However, high-fidelity methods are not always worth the cost. Therefore only propeller-wing interaction effects are mentioned for which a computationally efficient model is known.

It is expected that two-way coupling could affect propeller design. Two-way coupling could be included by including the effect of the wing on the propeller, since the local advance ratio on the blade sections change due to the wing induced upwash. Van Arnhem [29] developed a model that estimates the local change in advance ratio on the propeller blade due to the presence of another aerodynamic body. Furthermore, a weight model – that estimates propeller system weight based on performance – could further affect the optimization results. Wing bending alleviation could be aided by a propeller system, which perhaps means that the most optimized wing-propeller system does not return the most efficient propeller.

It is often suggested that propellers could have a beneficial effect on wing performance [7]. Inboard-up rotating wing-tip propellers are expected to reduce upwash, consequently reducing the effective angle of attack and induced drag. Including the propeller induced swirl velocites in the optimization process can more accurately calculate the drag force of the wing. A decrease in drag lowers the thrust requirement, eventually decreasing propeller power. Nederlof [18] describes the use of a slipstream tube model [25] with which the propeller induced velocities on the wing can be calculated. Such a wake model would be particularly well suited for rapid optimization since it is relatively inexpensive.

Acoustics have been identified as a key-factor in UAM development. If UAM technology is too disruptive, or loud, for urban environments it is likely that such UAM will not be employed on a large scale [30, 31]. Including an acoustic model could therefore be relevant for aeroacoustic UAM optimization.

VIII. Conclusion

Wing-propeller optimization can be achieved by using high fidelity models, however, high fidelity propeller-wing optimization is computationally expensive and may not be suitable during preliminary design phases. Therefore, an efficient coupled wing-propeller optimization process is needed for early aircraft design phases. Computationally efficient optimization is achieved by using inexpensive, yet sufficiently accurate, aerostructural models and the adjoint method.

This work presents a framework with which computationally efficient wing-propeller analysis and optimization is performed. Wing-propeller optimization with mid-fidelity requires specific implementation strategies. To couple the propeller to the wing, a slipstream model is necessary. However, the slipstream model affects the chosen wing-mesh, since the wing-mesh must satisfy certain slipstream requirements. Furthermore, the panels in a VLM require discrete velocities. Therefore, the propeller radius and location can not be included as design variables since this would require re-meshing and would cause discontinuities. Additionally, the current wing-propeller model would not benefit from propeller location as a design variable, since the slipstream model does not account for swirl, and thus the change in induced drag that the propeller causes on the wing. The coupled optimization also shows that the wing discretisation

affects the propeller design, since the slipstream velocities are only translated back to the wing as discrete points. In the future, a smoothing function should be used for the propeller velocity. Lastly, it is important to guarantee that the wing panels in- and outside the slipstream have approximately the same size, since the VLM could return non-physical results otherwise. The design philosophy of the framework was to build a modular architecture such that it is easily modifiable. Additional disciplines such as vehicle acoustics can easily be added, or current modules could be improved, if not replaced. The current iteration of the framework uses a modified version of OAS for wing aerostructural performance evaluation. Propeller performance is calculated using a BEMT code called HELIX. Lastly, the wing and propeller are coupled using a model developed by Rethorst. The coupled, and isolated, wing-propeller model numerical data showed good resemblance with experimental data. Furthermore, all of the code contains derivatives with implicit analytic methods, such as the adjoint method. The adjoint method is imperative for efficient gradient-based optimization since other methods such as finite differences experience a linear increase in cost, with an increase in design variables. Large systems, such as a propeller-wing system, with tens, if not hundreds, of design variables can therefore benefit from using implicit analytic methods.

The coupled optimization results were compared to those returned by isolated wing- and propeller-optimizations. Coupled optimization shows a 0.8% power decrease, as compared to isolated optimization. Furthermore, it was found that the wing discretisation affects the propeller optimization results. The propeller velocity distribution distribution is only translated to the wing at discrete points. Therefore the optimizer increased the velocity at those points, where it minimized the velocity at other points to decrease the power. This is not a physical phenomena and therefore it can be assumed that the propeller design is not optimal. To conclude, the completed framework, propeller model, wing model, and slipstream model show efficient wing-propeller optimization is possible. The optimization results show the significance of coupled optimization, which is a conservative estimate. Lastly, several recommendations are given that can provide further insights into the significance of propeller-wing optimization, as compared to isolated wing- and propeller-optimization.

IX. Acknowledgments

This research would not have been possible without the help of R. Nederlof, T. Sinnige and L. Veldhuis. They have provided continuous feedback on the material in this paper and the authors would like to express their gratitude for their help.

References

[1] Antcliff, K. R., Whiteside, S. K. S., Kohlman, L. W., and Silva, C., "Baseline Assumptions and Future Research Areas for Urban Air Mobility Vehicles," *AIAA Scitech 2019 Forum*, San Diego, California, 2019, pp. 1–18. doi:10.2514/6.2019-0528.

[2] Cole, J. A., Krebs, T. D., Barcelos, D. F., Yeung, A., and Bramesfeld, G., "On the Integrated Aerodynamic Design of a Propeller-Wing System," *AIAA Scitech 2019 Forum*, 2019, p. 2300.

[3] Clarke, M. A., Erhard, R. M., Smart, J. T., and Alonso, J., "Aerodynamic Optimization of Wing-Mounted Propeller Configurations for Distributed Electric Propulsion Architectures," *AIAA AVIATION 2021 FORUM*, 2021, p. 2471.

[4] Koyuncuoglu, H., and He, P., "Coupled Wing-propeller Aerodynamic Optimization Using the Adjoint Method," *AIAA SCITECH 2022 Forum*, 2022, p. 0015.

[5] Patterson, M. D., and German, B., "Conceptual Design of Electric Aircraft with Distributed Propellers: Multidisciplinary Analysis Needs and Aerodynamic Modeling Development," *52nd Aerospace Sciences Meeting*, AIAA, 2014. doi:10.2514/6.2014-0534.

[6] Martins, J. R. R. A., and Ning, A., *Engineering Design Optimization*, Cambridge University Press, 2021. doi:10.1017/9781108980647, URL `https://mdobook.github.io`.

[7] Sinnige, T., van Arnhem, N., Stokkermans, T. C. A., Eitelberg, G., and Veldhuis, L. L. M., "Wingtip-Mounted Propellers: Aerodynamic Analysis of Interaction Effects and Comparison with Conventional Layout," *Journal of Aircraft*, Vol. 56, No. 1, 2019, pp. 295–312. doi:10.2514/1.C034978.

[8] Martins, J. R. R. A., Sturdza, P., and Alonso, J. J., "The Complex-Step Derivative Approximation," *ACM Transactions on Mathematical Software*, Vol. 29, No. 3, 2003, pp. 245–262. doi:10.1145/838250.838251.

[9] Gray, J. S., Hwang, J. T., Martins, J. R. R. A., Moore, K. T., and Naylor, B. A., "OpenMDAO: An open-source framework for multidisciplinary design, analysis, and optimization," *Structural and Multidisciplinary Optimization*, Vol. 59, No. 4, 2019, pp. 1075–1104. doi:10.1007/s00158-019-02211-z.

[10] Lambe, A. B., and Martins, J. R. R. A., "Extensions to the Design Structure Matrix for the Description of Multidisciplinary Design, Analysis, and Optimization Processes," *Structural and Multidisciplinary Optimization*, Vol. 46, 2012, pp. 273–284. doi:10.1007/s00158-012-0763-y.

[11] Gill, P. E., Murray, W., and Saunders, M. A., "SNOPT: An SQP Algorithm for Large-Scale Constrained Optimization," *SIAM Review*, Vol. 47, No. 1, 2005, pp. 99–131. doi:10.1137/S0036144504446096.

[12] Wu, N., Kenway, G., Mader, C. A., Jasa, J., and Martins, J. R. R. A., "pyOptSparse: A Python framework for large-scale constrained nonlinear optimization of sparse systems," *Journal of Open Source Software*, Vol. 5, No. 54, 2020, p. 2564. doi:10.21105/joss.02564.

[13] Jasa, J. P., Hwang, J. T., and Martins, J. R. R. A., "Open-source coupled aerostructural optimization using Python," *Structural and Multidisciplinary Optimization*, Vol. 57, No. 4, 2018, pp. 1815–1827. doi:10.1007/s00158-018-1912-8.

[14] Pacini, B., Yildirim, A., Davoudi, B., Martins, J. R. R. A., and Duraisamy, K., "Towards Efficient Aerodynamic and Aeroacoustic Optimization for Urban Air Mobility Vehicle Design," *AIAA Aviation Forum 2021*, 2021. doi:10.2514/6.2021-3026.

[15] Rethorst, S., "Aerodynamic of Nonuniform Flows as Related to an Airfoil Extending Through a Circular Jet," *Journal of the Aerospace Sciences*, Vol. 25, No. 1, 1958, pp. 11–28.

[16] Nederlof, R., "Improved modeling of propeller-wing interactions with a lifting-line approach: Investigation of a suitable correction method to account for the finite slipstream height," 2020.

[17] Willemsen, R., "A Sensitivity Study on the Aerodynamic Performance of a Wingtip-Mounted Tractor Propeller-Wing System," Master's thesis, Delft University of Technology, 2020.

[18] Nederlof, R., Kooij, R., Veldhuis, L. L., and Sinnige, T., "Contribution of Swirl Recovery to the Induced Drag of a Propeller-Wing System–A Parametric Study," *AIAA AVIATION 2023 Forum*, 2023, p. 3543.

[19] Van der Leer, Q., and Hoogreef, M., "Aero-Propulsive and Aero-Structural Design Integration of Turboprop Aircraft with Electric Wingtip-Mounted Propellers," *AIAA SCITECH 2022 Forum*, 2022, p. 0167.

[20] Amos, D. E., "Algorithm 644: A Portable Package for Bessel Functions of a Complex Argument and Nonnegative Order," Vol. 12, No. 3, 1986. doi:10.1145/7921.214331, URL https://doi-org.tudelft.idm.oclc.org/10.1145/7921.214331.

[21] Prabhu, R. K., "Studies on the interference of wings and propeller slipstreams," 1984.

[22] van der Leer, Q., "A review of the wingtip-mounted propeller configuration," Master's thesis, Delft University of Technology, 2020.

[23] Raymer, D. P., *Aircraft Design: A Conceptual Approach*, 4th ed., AIAA, 2006.

[24] Sethi, S., Striz, A., Sethi, S., and Striz, A., "On using the Kreisselmeier-Steinhauser function in simultaneous analysis and design," *38th Structures, Structural Dynamics, and Materials Conference*, 1997.

[25] Veldhuis, L. L. M., "Propeller Wing Aerodynamic Interference," Ph.D. thesis, Delft University of Technology, 2005.

[26] Lyu, Z., Kenway, G. K. W., and Martins, J. R. R. A., "RANS-based Aerodynamic Shape Optimization Investigations of the Common Research Model Wing," *Proceedings of the AIAA Science and Technology Forum and Exposition (SciTech)*, National Harbor, MD, 2014. doi:10.2514/6.2014-0567, aIAA 2014-0567.

[27] Kaneko, S., and Martins, J. R. R. A., "Simultaneous Optimization of Conceptual Design and Takeoff Trajectory of a Lift-Plus-Cruise UAV," *10th Autonomous VTOL Technical Meeting*, 2023.

[28] Chauhan, S. S., and Martins, J. R. R. A., "Low-Fidelity Aerostructural Optimization of Aircraft Wings with a Simplified Wingbox Model Using OpenAeroStruct," *Proceedings of the 6th International Conference on Engineering Optimization, EngOpt 2018*, Springer, Lisbon, Portugal, 2018, pp. 418–431. doi:10.1007/978-3-319-97773-7_38.

[29] N. van Arnhem, T. S. R. V. G. E., R. de Vries, and Veldhuis, L. L. M., "Engineering method to estimate the blade loading of propellers in nonuniform flow," *AIAA Journal*, 2020.

[30] Johnson, W., Silva, C., and Solis, E., "Concept Vehicles for VTOL Air Taxi Operations," *Proceedings of the AHS technical conference on Aeromechanics Design for Transformative Vertical Flight*, 2018.

[31] Moore, M. D., "Personal Air Vehicles: A Rural/Regional and Intra-Urban On-Demand Transportation System," *Journal of the American Institute of Aeronautics and Astronautics (AIAA)*, AIAA, Dayton, Ohio, 2003, pp. 1–20.